Polariton formation in functionalized tetracene for manipulating excited states dynamics and photochemistry

Roshell Lamug[a], Winston T. Goldthwaite[a], John E. Anthony[b], and Oksana Ostroverkhova[a]

[a]Department of Physics, Oregon State University, Corvallis, OR 97331
[b]Department of Chemistry, University of Kentucky, Lexington, KY 40506

ABSTRACT

Understanding singlet fission, a charge carrier multiplication process, and how the singlet fission and the competing processes can be manipulated with external parameters within the same material system is of considerable interest for enhancing optoelectronic device performance. Exciton polaritons, formed by strong exciton-photon coupling in organic films in microcavities, have been shown to manipulate the energy landscape that may be used to control the photophysics and photochemistry in existing singlet fission materials. To efficiently utilize exciton polariton formation to enhance singlet fission and suppress competing processes such as relaxation into low-energy trap states, it is necessary to establish how the properties of polaritons in singlet fission materials depend on molecular photophysics and microcavity configurations. We present a systematic study of strong coupling in functionalized tetracene (R-Tc), and how it affects its photophysics and photochemistry, depending on film morphology, placement in the cavity (to achieve various degrees of overlap with the cavity electric field), and cavity design. We probe cavity-coupled and uncoupled molecular populations and examine the effects of intermolecular interactions on the excited state dynamics and polariton formation and properties. By varying magnetic field, we create different excited states relaxation scenarios and determine how the polariton states participate in the competition between the singlet fission and relaxation into trap states. We observe magnetic field-enhanced emission from exciton and polariton states and cavity-suppressed emission from low-energy trap states. We also report on effects of polariton formation on photodimerization of R-Tc and discuss how concurrent studies of photochemistry and photophysics promote understanding of singlet fission and polariton formation through the evolution of excited states during photodegradation.

Keywords: Organic semiconductors, singlet fission, exciton polaritons, photodimerization

1. INTRODUCTION

Organic (opto)electronic materials are of interest due to their low cost and tunable properties, with applications ranging from photovoltaics to display technologies demonstrated and commercialized.[1] There has been considerable progress in organic device performance across various device platforms, due to an improved understanding of mechanisms and structure-property relationships which have guided the design of organic materials with enhanced optoelectronic characteristics, with, for example, solar cells power conversion efficiencies (PCEs) approaching 20%.[2] One important process for further improvement of both all-organic and organic-inorganic hybrid solar cells is singlet fission (SF), a carrier multiplication process in which one absorbed photon generates two pairs of mobile charge carriers and enables PCEs that surpass the Schockley-Quiesser theoretical limit on solar cell efficiency. However, in spite of much improved understanding of the SF mechanisms, utilizing SF in devices has been challenging due to a number of constraints on the molecular energies and photophysics, which limits the choices for the successful systems. One promising way to mitigate some of these limitations is by utilizing light-matter hybrid states (polaritons) to modify excited-state energies and dynamics towards relaxing these constraints.[3]

Another critical obstacle for commercializing organic electronics is the limited (photo)stability of organic materials. Polariton chemistry is an emerging area that aims to control (photo)chemical reactions, offering a

Further author information: (Send correspondence to O.O.)
E-mail: oksana@science.oregonstate.edu, Telephone: 1 541 737 1679

Physical Chemistry of Semiconductor Materials and Interfaces XXIII, edited by Andrew J. Musser, Loreta A. Muscarella, Proc. of SPIE Vol. 13127, 131270D
 · 0277-786X · doi: 10.1117/12.3028145

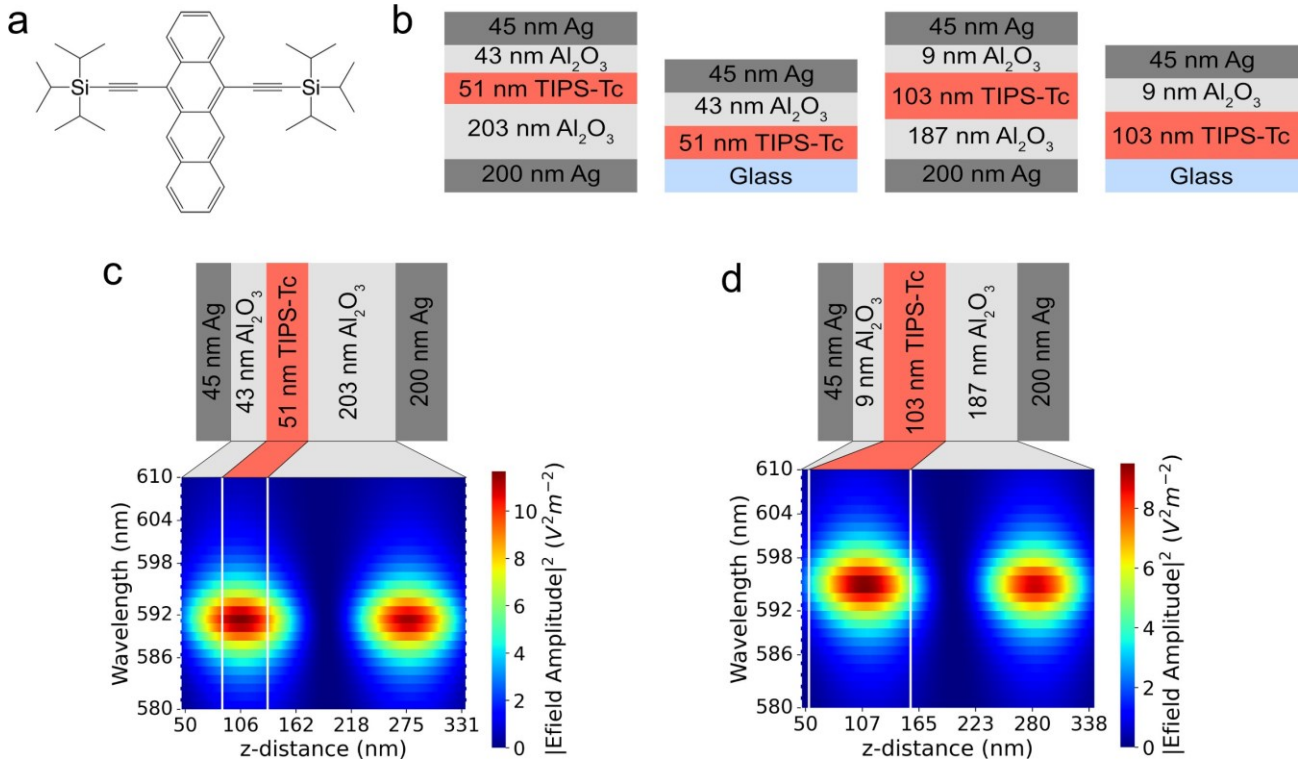

Figure 1. (a) Molecular structure of TIPS-Tc. (b) Schematic of optical planar microcavities and their corresponding 'top' samples used as a control. Squared electric field of the (c) 51 nm and (d) 103 nm microcavities at normal incidence modelled by TMM. The microcavities are tuned such that the TIPS-Tc layer is adjusted to the maximum of the electric field by the use of spatial layers of aluminum oxide.

way to enhance both performance and stability of organic optoelectronics.[3] Therefore, it is important to understand how the polariton formation affects both photophysics and photochemistry of benchmark SF materials and what current challenges can be mitigated using polaritons. In this paper, we examine a benchmark SF material, functionalized tetracene derivative TIPS-Tc, incorporated into microcavities and establish photophysical and photochemical characteristics of TIPS-Tc under strong coupling conditions (i.e., in the presence of polaritons). In particular, we investigate how the excited states of TIPS-Tc are affected by strong coupling of the TIPS-Tc excitons to the cavity photons at different magnetic fields and temperature, depending on the cavity characteristics, and examine photodegradation via photodimerization under strong coupling conditions.

2. EXPERIMENTAL

2.1 Materials and Sample Preparation

In our experiments, we used blends of tetracene (Tc) derivative functionalized with a side group of 5,12-Bis((triisopropylsilyl)ethynyl) (TIPS) (Figure 1(a)) with poly(methyl methacrylate) (PMMA) such that the average intermolecular spacing between R-Tc molecules d = 1 nm.[4] To create different thicknesses of films, while keeping the same average intermolecular spacing, different concentrations of PMMA were combined with TIPS-Tc at different concentrations. For example, to make thinner TIPS-Tc films of 51 nm, a 5 mg/mL toluene solution of PMMA was combined with 13.35 mM of TIPS Tc. To fabricate the thicker 103 nm films, 30 mg/mL toluene solution of PMMA was combined with 80.13 mM of TIPS-Tc.

A range of film thicknesses was chosen to create λ-thick microcavities with varying resonance frequencies and electric field overlap. To fabricate strongly coupled microcavities, 200 nm of Ag is thermally evaporated onto a glass substrate. To control placement of the TIPS-Tc layer in the maximum of the cavity electric field, and to

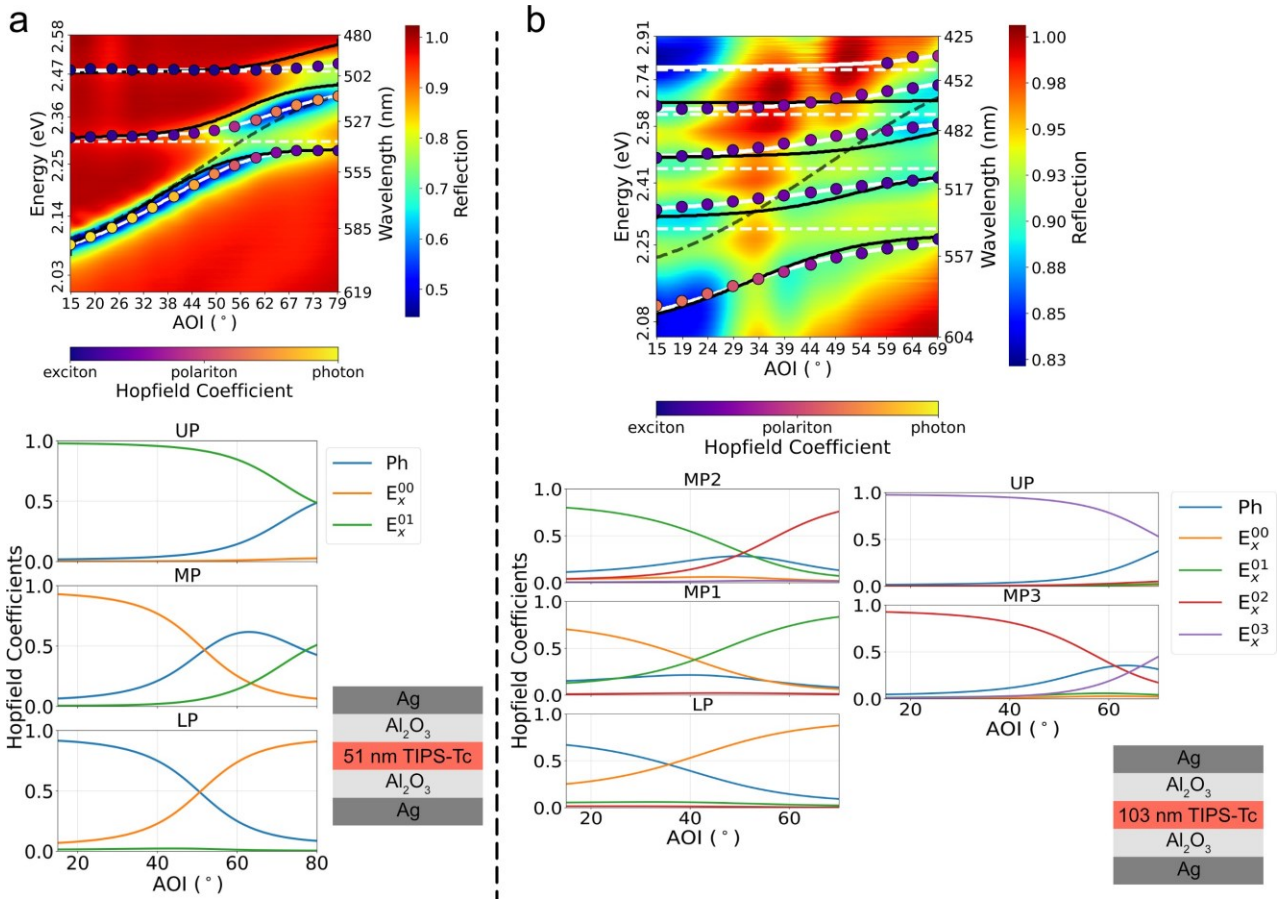

Figure 2. Polariton dispersion and Hopfield coefficients for (a) 51 nm cavity, and (c) 103 nm cavity. Dashed black line is the cavity photon energy. Heat maps are experimentally measured angle-resolved reflectance data. Data points are the reflectance dip energies, taken as described in Section 2.2, colored to match the polariton state's photonic component. Solid white lines are the fits of the data to the coupled oscillators model while the black solid lines are the fitted TMM-simulated data. Measured bare exciton energies are depicted with dashed white lines.

tune the energy of the cavity photon, spatial layers are used above and below the TIPS-Tc layer. The spatial layers are made of Al_2O_3 ranging from 9-203 nm and were fabricated by atomic layer deposition (Veeco Savannah S200 ALD). The TIPS-Tc layer is spincast at various speeds to achieve active layers of 51 nm and 103 nm. The cavity is then finished with 45 nm of thermally evaporated Ag. Control 'top' samples that have no strong coupling are similarly made, with the TIPS-Tc layer spincast on glass at the same speed as its cavity counterpart, Al_2O_3 films added by atomic layer deposition, and samples finished with 45 nm of thermally evaporated Ag. Samples will be referred to by their TIPS-Tc:PMMA layer thickness, i.e. "103 nm" or "51 nm" 'top' sample/cavity.

2.2 Measurements

Angle-resolved reflectance (ARR) for all cavities, illuminated by s-polarized light at angles of incidence between 15° and 80° in 5° steps, was measured using a custom built optical assembly. White light from a fiber-coupled tungsten filament source was passed through a linear polarizer before being focused onto the sample at different angles of incidence. Reflected light was then collected and analyzed using an Ocean Optics USB2000-FLG spectrometer. The center energies of the cavity reflection resonances were modeled by using a coupled oscillators model for polaritons as described our previous publications.[4,5]

The electric field strength and ARR of the cavities were simulated using the transfer matrix method (TMM). Models of the cavities were prepared as semi-infinite air / 45 nm of Ag / Z1 nm of Al_2O_3 / L nm of TIPS-Tc

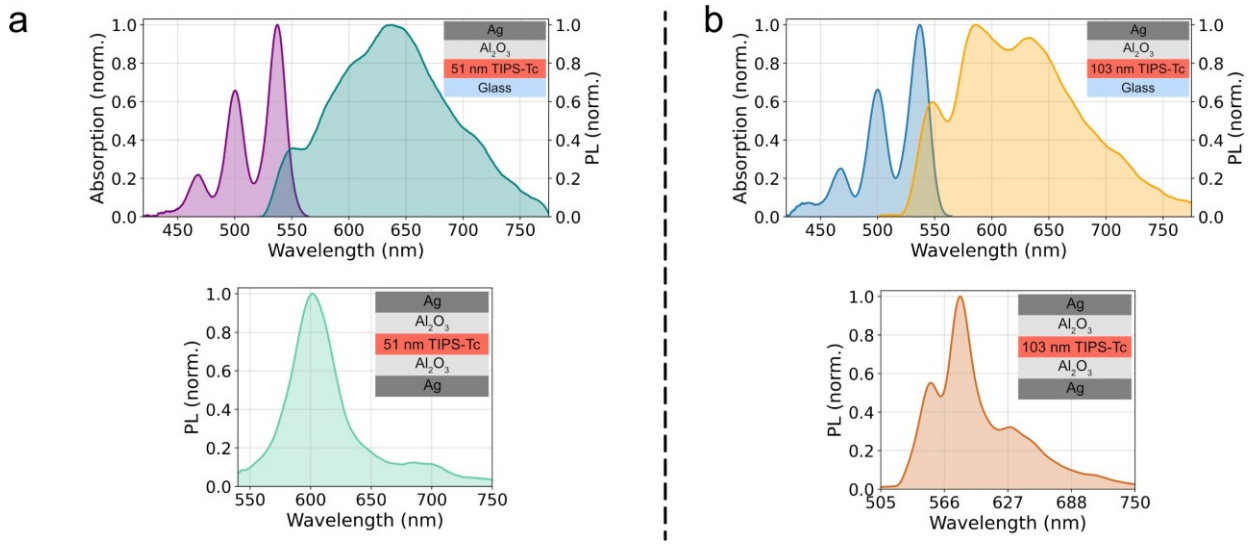

Figure 3. Photoluminescence and absorption of (a) 51 nm 'top' and (b) 103 nm 'top' samples. Under their corresponding 'top' sample, the PL obtained at normal incidence of (a) 51 nm cavity and (b) 103 nm cavity is shown. The 51 nm cavity shows primarily lower polariton emission while the 103 nm cavity emission shows considerable contribution from uncoupled emissive populations.

/ Z2 nm of Al_2O_3 / 200 nm of Ag / semi-infinite BK7 glass, where L is the thickness of the TIPS-Tc film and Z1/Z2 is the thickness of the Al_2O_3 film on the top/bottom of the TIPS-Tc film. The thicknesses for each film are indicated in Figure 1(b). For each system, a normalized plane wave of 400-900 nm at angles of incidence between 0°-90° was used together with the TMM to calculate the total reflectance of the system and the field internal to each layer as a function of wavelength. The field intensity was then calculated as a function of depth within the system. Figures 1(c-e) show the calculated distribution of the squared electric field over the layers of the cavity at normal incidence. The simulated ARR are shown by the black solid lines in Figures 2(a-c) to compare to measured results.

After the ARR was characterized, the samples were placed in a magneto-optic cryostat (OptiCool, Quantum Design, Inc.) for magnetic-field- (B-field) and temperature-dependent measurements. For optical absorption measurements in the cryostat, samples were illuminated by a tungsten halogen lamp focused onto the sample with a 10x objective to a near diffraction-limited spot (<5 μm). The reflection was collected and measured using a SpectraPro HRS-300 spectrograph. Photoluminescence (PL) of the samples was measured using either 450 nm or 515 nm excitation from 100-180 fs pulses at 10 kHz from a second-harmonic generation system (SHG, APE HarmoniXX), pumped by femtosecond pulses at 10 kHz from an optical parametric amplifier (OPA, ORPHEUS-F, Light Conversion). The excitation beam was focused on the sample and the PL was collected as in measurements of absorption, after filtering the excitation beam using a 500 nm long-pass or a 550 nm long-pass filter.

To induce photodegradation via photodimerization,[6] the 51 nm TIPS-Tc cavity was placed in the magneto-optic cryostat and illuminated by a 532 nm continuous wave laser (frequency-doubled Nd:YVO4, Verdi-5, Coherent, Inc.) at 300 K. The excitation beam was focused on the sample and the PL was collected as in measurements of absorption, with 550 nm long-pass filter. Photodegradation was measured from two different spots on the sample at 0 T and 6T external magnetic field.

3. RESULTS AND DISCUSSION

3.1 Strong coupling in microcavities

The ARR of the TIPS-Tc microcavities exhibited anti-crossing behavior and dispersion (Figure 2(a-c)), characteristic of exciton polaritons. The 103 nm cavity shows four exciton transitions (0-0, 0-1, 0-2, 0-4) within

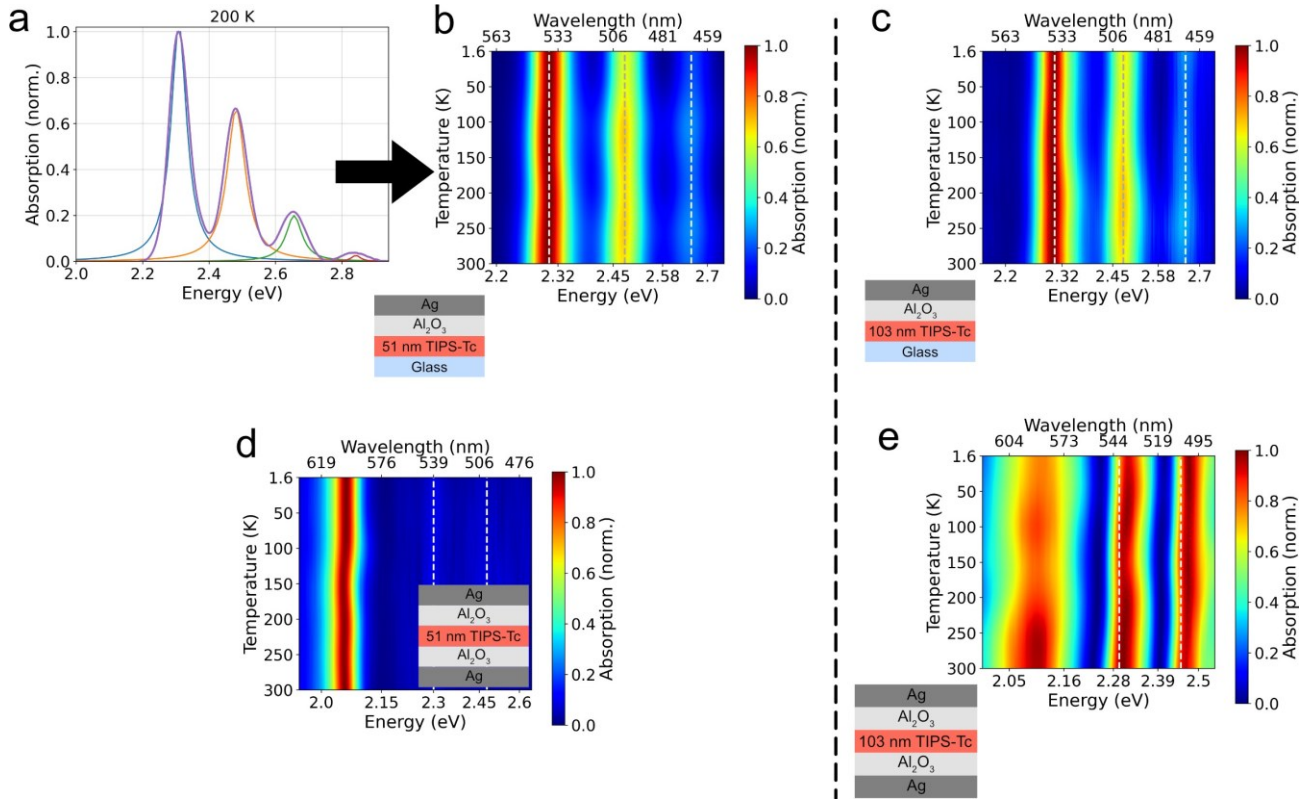

Figure 4. Optical absorption of 'top' and cavity samples at temperatures in the 1.6 K - 300 K range. (a) Normalized absorption spectrum at 200K for the 51 nm 'top' sample; Lorentzian fits of the vibronic progression are also included. (b)-(e) Normalized absorption spectra as a function of temperature for (b) 51 nm 'top' sample, (c) 103 nm 'top' sample, (d) 51 nm cavity, and (e) 103 nm cavity, with dashed lines indicating the exciton energies.

the S_0-S_1 absorption band of the TIPS-Tc film coupled to the cavity photon creating the lower polariton (LP), three middle polariton (MP1, MP2, and MP3), and the upper polariton (UP) branches. The exciton-photon interaction strengths $2V_{0m}$ obtained from the coupled oscillator model fits yielded 228 meV, 200 meV, 158 meV, and 128 meV for the 0-n (n = 0-3) transitions, and a cavity detuning of -97 meV. The thinner 51 nm cavity yielded interaction strengths less than half of those of the 103 nm cavity and showed coupling only to the first two exciton transitions, with $2V_{0m}$ of 90 meV and 66 meV for the 0-0 and 0-1 transitions, respectively. Parameters for the coupled oscillator model fit can be found in Table 1.

The thinner cavities were tuned such that the 51 nm cavity LP is 10 nm redshifted (600 nm) from that of the 103 nm cavity LP (590 nm). Hopfield coefficients at normal incidence show that the LP is 67% and 95% photonic for the 103 nm and 51 nm cavities, respectively. With different thicknesses of TIPS-Tc in the maximum of the cavity electric field, the varying fractions of the excitonic and photonic components of the LP and different detunings are used to probe how polaritons interact with uncoupled molecular populations.

3.2 Photoluminescence

The optical absorption and PL of the 'top' samples are summarized in Figure 3. The optical absorption spectra are similar to those of TIPS-Tc molecules in a dilute solution,[6] which suggests that the TIPS-Tc:PMMA blends under study are amorphous. The PL spectra depend on the film thickness and have different relative yields of "550 nm"-, "580 nm"-, "630 nm"-, and "700 nm"-dominated spectral features. Both 'top' samples have a minor "550 nm" emission, which aligns with a S_1 0-0 transition of TIPS-Tc. In the 51 nm 'top' sample in Figure 3(a), PL is dominated by the "630 nm" peak; this feature was previously assigned to an excimer[7] or the entangled triplet-pair ('(TT)) state in disordered films[8] in TIPS-Tc and to physical dimer-like trap states in films of other

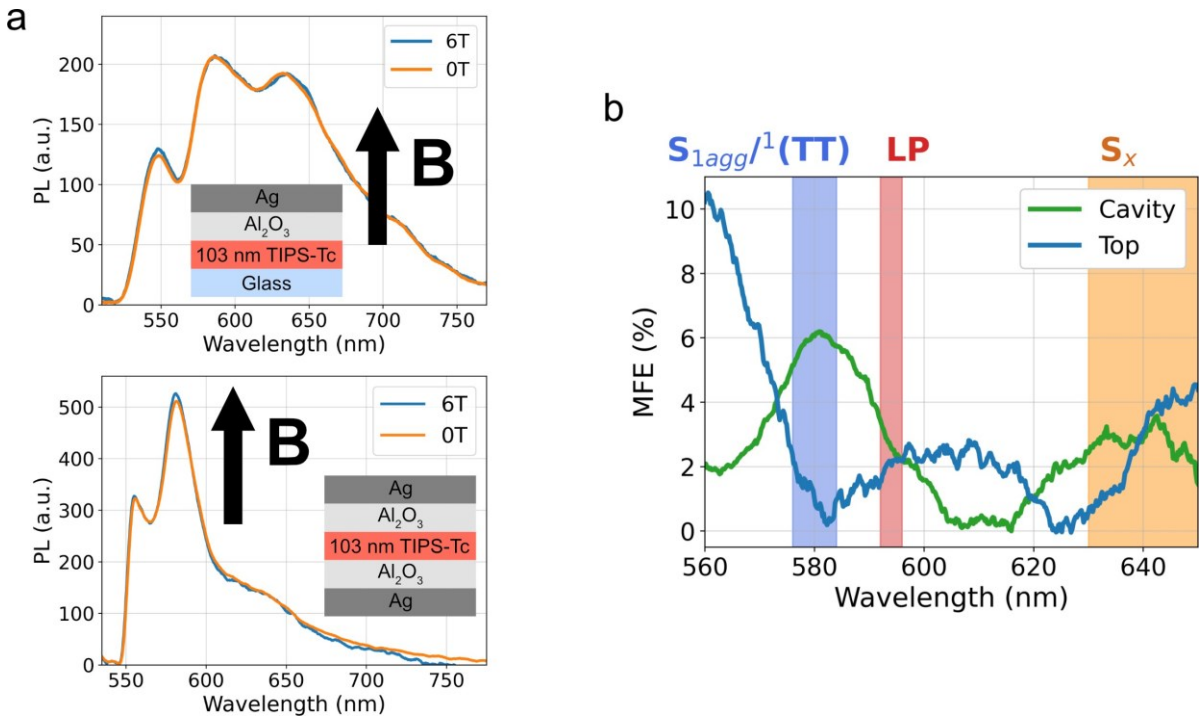

Figure 5. (a) Tracking PL under 0 T ant 6 T external magnetic field (B) taken at 300 K under 515 nm excitation. (b) Magnetic field effect (MFE) of the 103 nm top and cavity sample taken at 300 K under 515 nm excitation. MFE = (PL(B = 6 T) - PL(B = 0 T))/PL(B = 0 T). Colored in regions overlayed on the plot note the wavelength ranges of emissive populations.

R-Tc derivatives.[9] The ”580 nm” spectral feature, which dominates the PL spectrum of the 103 nm ’top’ sample, is located where the emission of either the relaxed S_1 exciton (e.g., aggregate emission S_{1agg})[9] or the ^{1}(TT) state in polycrystalline TIPS-Tc films[8] would emit. This ”580 nm” spectral feature will be referred to as $S_{1agg}/^1$(TT). Both films have emission extended to near-infrared wavelengths (>700 nm), referred to as ”700 nm” emission, due to low-energy trap states which will be referred to as Sx.

When these films are placed in the microcavites, a suppression of specific spectral features is observed. The 51 nm cavity emission (Figure 3(a),bottom) is dominated by that from the LP at 600 nm and shows suppression of all ’top’-sample spectral features. This is expected, since there is a strong overlap between the electric field and the thin TIPS-Tc layer (Fig. 1(c)), and so most of the molecules present in the cavity undergo efficient strong coupling. In contrast, the thicker TIPS-Tc film in the 103 nm cavity has a smaller fraction of molecules that strongly couple and form polaritons (Fig. 1(d)). As a result, the 103 nm cavity emission (Figure 3(b),bottom) has a considerable contribution from the uncoupled molecules similar to those in the ’top’ sample. It is dominated by the S1agg/^{1}(TT)/LP emission at 580-590 nm, but with a reduced contribution of the ”630 nm” and ”700 nm” features from the low-energy states. The presence of both polariton emission and exciton emission from uncoupled molecules is attractive for probing of both molecular populations within the same cavity.

3.3 Temperature dependence of optical absorption

The optical absorption of all samples was measured from 300 K to 1.6 K in 50 K increments. Each absorption spectrum was fitted with Lorentzians to track the peak locations and linewidths as a function of temperature. Example of such fits to the 0-n (n = 0-3) vibronic lines is shown in Fig. 4(a). The resulting normalized absorption as a function of temperature is shown in Figure 4. All samples show a slight blueshift in absorption peak energies as the temperature decreases and a temperature-independent linewidths in their absorption spectra. The ’top’ samples exhibit a blueshift within 1 nm, while the LP feature in the microcavities has a 3 nm blueshift as the

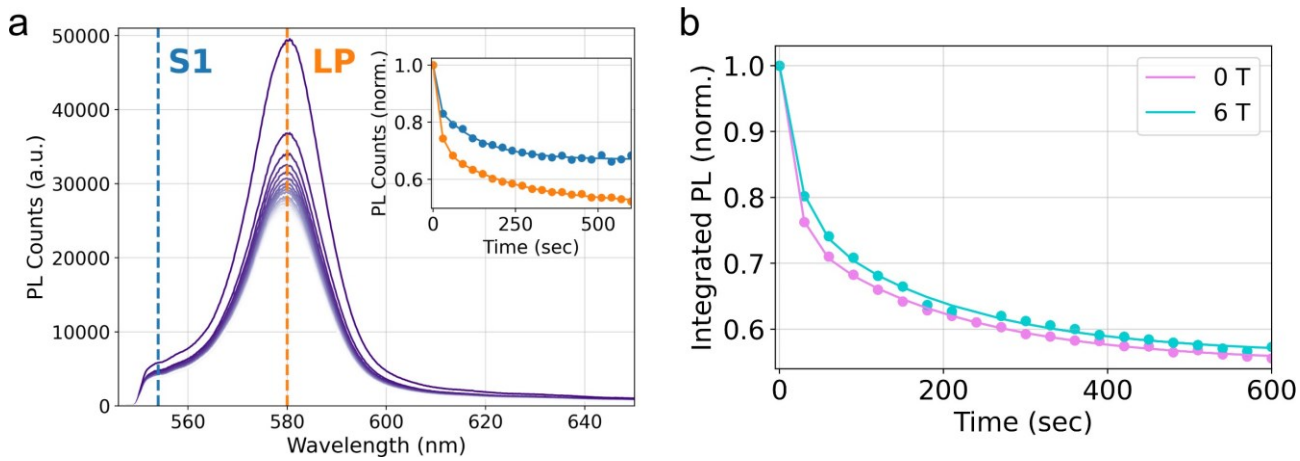

Figure 6. (a) Evolution of PL from 51 nm cavity with 580 nm LP resonance under continuous exposure to 532 nm excitation due to photodimerization. Right inset: time evolution of the PL of S_1 (blue) and LP state (orange), normalized at its value at time t = 0. (b) Integrated PL under continuous exposure to 532 nm excitation at 0 T (pink) and 6 T external B-field (blue) (data points). Biexponential fits to the data in the inset of (a) and in (b) are shown as solid lines, with fit parameters included in Table 2.

temperature is lowered from 300 K to 1.6 K. This blueshift is an indication of thermal contraction of the TIPS-Tc:PMMA layer which results in an overall blueshift of the cavity resonance and a change in detuning. The change in detuning shifts the LP branches in the 300 K - 1.6 K temperature range from 95% to 94% photonic character for the 51 nm cavity and 67% to 61% photonic character for the 103 nm cavity at normal incidence.

3.4 Magnetic field effects (MFEs) in emission

To study how polariton states participate in the competition between singlet fission (SF) and other relaxation pathways such as relaxing into trap states, the thicker cavity was chosen to probe any magnetic field (B-field)-induced spectral changes in coupled and uncoupled molecule emission compared to those in the corresponding 'top' sample. The PL of the 103 nm 'top' and cavity samples was measured under a 0 T and a 6 T external B-field. Strong B-fields affect the dissociation of the '(TT) states into weakly correlated triplet pairs (T..T), thus decreasing SF rates, leading to an enhanced PL emission.[9, 10] This effect is especially pronounced at higher temperatures,[9] and, consistent with these expectations, at 300 K under 6 T, we observed an increase in PL in both 'top' and cavity samples (Figure 5(a)) as compared to that at 0 T. The wavelength dependent MFE was then calculated using the MFE = (PL(B = 6 T) - PL(B = 0 T))/PL(B = 0 T) and is shown in Figure 5(b) for the 103 nm 'top' and cavity samples.

In the 'top' sample, the S_1 "550 nm" emission experiences the strongest MFE of 10%. This suggests that this state has the strongest kinetic connection to the SF process, which is depopulated by the '(TT) formation and repopulated by triplet fusion from '(TT), which is enhanced when the '(TT) dissociation is impeded by the B-field. The lower-energy emissive states have kinetic connections to the '(TT) states via S_1, but these connections are weaker and thus, MFEs are weaker as well.[9] Interestingly, in the cavity, the 580-590 nm emission from the S1agg/'(TT)/LP states has the strongest MFE (~6%), which suggests that the cavity coupling modifies the S_1 relaxation dynamics and the energy landscape such that the states emitting from the lower-energy 580-590 nm states have a stronger kinetic connection to the SF process than higher-energy 550 nm-emitting S_1 state.

3.5 Photodegradation experiments

Next, we investigate how the photodegradation via photodimerization[6] affects different emissive states. For this, we examined a thinner cavity with PL dominated by LP emission exposed to continuous 532 nm illumination. In addition to the importance of understanding the photochemistry responsible for degradation, it can provide insight into excited states involved in intermolecular processes like SF.[11] To explore possible connections between the SF, polariton formation, and photodimerization, one spot in the 51 nm cavity with LP at 580 nm is

photobleached in vacuum at 0 T (Fig. 6(a)), and then the experiment is repeated on a different spot on the same cavity with the same LP energy at 6 T. At 0 T, the photodimerization rates for the residual ”550 nm” S_1 emission and 580 nm LP emission are also analyzed separately, with an integrated emission of each feature shown in the inset of Figure 6(a). The integrated PL obtained at 0 T and 6 T during the photodimerization is shown in Figure 6(b), with bi-exponential fits included in the figure and fit parameters summarized in Table 2.

The photodegradation of TIPS-Tc molecules in the microcavity translates into a large monotonic decrease of emission from all states, but with different rates and the fractions of the population not susceptible to photodimerization (given by the parameter A_0 in Table 2). In particular, a considerably higher molecular population that emits via LP is in molecular configurations conducive to photodimerization (48%) (Table 2) as compared to that emitting via S_1 (33%). Because the photodimerization is known to proceed via an excimer precursor, formed either from S_1 or ^{1}TT (e.g., $S_0+S_1 \rightarrow$ excimer $\rightarrow$ dimer) or (^{1}(TT) $\rightarrow$ excimer $\rightarrow$ dimer),[12] this may indicate that the states emitting through LP are also those that form such excimer states more efficiently. With the strong B-field slowing down the degradation (Fig. 6(b) and Table 2), it is possible that the excimer potential energy surfaces are modified with the B-field to increase the barrier for photodimerization.

4. CONCLUSIONS

In summary, we investigated how strong coupling affects photophysics and photochemistry in a benchmark SF material, TIPS-Tc, when placed in microcavities. Two microcavities with different active TIPS-Tc layer thicknesses, characterized by coupling strengths $2V_{00}$ of 90 meV and 228 meV, were investigated at various temperatures and B-fields, side by side with control ’top’ samples. The cavity featuring a thinner TIPS-Tc film exhibits predominantly the LP emission, while the cavity with a thicker TIPS-Tc film shows both LP and exciton emission. As temperature decreases from 300 K to 1.6 K, the polariton energies exhibit a 3 nm blueshift due to thermal contraction affecting cavity resonance, which results in a small temperature-dependent change in the photonic/excitonic character of polaritons. B-field dependent PL shows a shift from the strongest MFE of S_1 ”550 nm”-emitting state in ’top’ samples to that of lower-energy S1agg/^{1}TT/LP 580-590 nm-emissive state, indicative of a shift in the energy landscape for the states with the strongest kinetic connection to the SF process. Photodimerization in cavities yielded different photodimerization rate constants for different molecular populations. The population emitting via LP was more susceptible to photodegradation via photodimerization than the S_1-emitting population, and the photodegradation proceeded slower at strong B-fields.

APPENDIX A. COUPLED OSCILLATOR MODEL PARAMETERS

Table 1. Fit parameters for a coupled oscillator model[5] applied to simulated and measured angle-resolved reflectance data for the two cavities, obtained as described in Section 2.2. The difference in the exciton energy E_X^{00} and photon energy E_0 at normal incidence is described as the detuning, Δ.

		E_0 [eV]	n_{eff}	$2V_{0i}$ [meV] (E_X^{0i} [eV])				Δ [meV]
				i = 0	i = 2	i = 3	i = 4	
103 nm TIPS-Tc Cavity	Measured	2.19	1.64	228 (2.289)	200 (2.450)	158 (2.619)	128 (2.779)	-97
	Simulated	2.11	1.76	146 (2.295)	138 (2.469)	70 (2.657)		-181
51 nm TIPS-Tc Cavity	Measured	2.11	1.93	102 (2.298)	90 (2.470)			-184
	Simulated	2.09	1.77	110 (2.296)	98 (2.467)			-209

APPENDIX B. BI-EXPONENTIAL FIT PARAMETERS FOR PHOTODEGRADATION

ACKNOWLEDGMENTS

This work was supported by the National Science Foundation (NSF) (CHE-1956431). Sample fabrication and characterization was partially performed in NSF-funded user facilities via NNCI:NNI EECS-2025489 and MRI

Table 2. Fit parameters for the time evolution of normalized total integrated PL, 550 nm, and 580 nm PL features ($A_1exp(-k_1t)+ A_2exp(-k_2t)+A_0$, with $A_0 + A_1 + A_2 = 1$) obtained under the same irradiation conditions as described in Section 2.2.

		A_1	$k1\ (s^{-1})$	A_2	$k2\ (s^{-1})$	A_0
0 T	Integrated	0.244	0.063	0.206	0.0051	0.550
	550 nm	0.128	0.199	0.203	0.0079	0.669
	580 nm	0.282	0.057	0.203	0.0045	0.515
6 T	Integrated	0.214	0.047	0.224	0.0053	0.562

DMR-1920368 grants.

REFERENCES

[1] Ostroverkhova, O., "Organic optoelectronic materials: Mechanisms and applications," *Chem. Rev.* **116**, 13279–13412 (2016).

[2] Fu, J., Yang, Q., Huang, P., Chung, S., Cho, K., Kan, Z., Liu, H., Lu, X., Lang, Y., Lai, H., He, F., Fong, P. W. K., Lu, S., Yang, Y., Xiao, Z., and Li, G., "Rational molecular and device design enables organic solar cells approaching 20% efficiency," *Nat. Commun.* **15**, 1830 (2024).

[3] Bhuyan, R., Mony, J., Kotov, O., Castellanos, G. W., Rivas, J. G., Shegai, T. O., and Borjesson, K., "The rise and current status of polaritonic photochemistry and photophysics," *Chem. Rev.* **123** (2023).

[4] Schenck, J. D. B. V., Goldthwaite, W. T., Puro, R., Anthony, J., and Ostroverkhova, O., "Exciton polaritons reveal "hidden" populations in functionalized pentacene films," *J. Phys. Chem. C* **125**, 27381–27393 (2021).

[5] Schenck, J. D. B. V., Tanyi, E. K., Cheng, L.-J., Anthony, J., and Ostroverkhova, O., "Strong exciton–photon coupling in anthradithiophene microcavities: from isolated molecules to aggregates," *MRS Comm.* **9**, 956–963 (2019).

[6] Puro, R., Schenck, J. D. B. V., Center, R., Holland, E. K., Anthony, J. E., and Ostroverkhova, O., "Exciton polariton-enhanced photodimerization of functionalized tetracene," *J. Phys. Chem. C* **125**, 27072–27083 (2021).

[7] Dover, C. B., Gallaher, J. K., Frazer, L., Tapping, P. C., II, A. J. P., Crossley, M. J., Anthony, J. E., Kee, T. W., and Schmidt, T. W., "Endothermic singlet fission is hindered by excimer formation," *Nat. Chem.* **10**, 305–310 (2018).

[8] Stern, H. L., Cheminal, A., S. R. Yost, K. B., Bayliss, S. L., Chen, K., Tabachnyk, M., Thorley, K., Greenham, N., Hodgkiss, J. M., Anthony, J., Head-Gordon, M., Musser, A. J., Rao, A., and Friend, R. H., "Vibronically coherent ultrafast triplet-pair formation and subsequent thermally activated dissociation control efficient endothermic singlet fission," *Nat. Chem.* **9**, 1205–1212 (2017).

[9] Goldthwaite, W. T., Lambertson, E., Gragg, M. E., Anthony, J. E., Zuehlsdorff, T., O., and Ostroverkhova, "Morphology-dependent singlet fission and photodegradation in functionalized tetracene crystals and films," *Submitted* (2024).

[10] Burdett, J. J., Piland, G. B., and Bardeen, C. J., "Magnetic field effects and the role of spin states in singlet fission," *Chem. Phys. Lett.* **585**, 1–10 (2013).

[11] Goldthwaite, W., Chase, M., Gragg, M., Lamug, R., Windemuller, D., Parkin, S., Anthony, J. E., and Ostroverkhova, O., "Elucidating photophysics-photochemistry relationship in singlet fission materials," *MRS Adv.* **9**, 707–714 (2024).

[12] Charlton, J. L., Dabestani, R., and Saltiel, J., "Role of triplet-triplet annihilation in anthracene dimerization," *J. Am. Chem. Soc.* **105**, 3473–3476 (1983).